differences between terminal and bridging sites, while suggesting steric contributions to the overall reactivities, in no way accounts for the overall sluggishness of these reactions. Other structural and electronic factors of substrate and solvent must play the dominant roles in explaining these features.

Acknowledgment. This work was supported by a U.S. Department of Energy (Office of Basic Energy Sciences) contract to PCF and by a National Science Foundation grant to R.G.P.

Registry No. CH_3O^-, 3315-60-4; CH_3OH, 67-56-1; $H_4Ru_4(CO)_{11}[P(OMe)_3]$, 34438-92-1; $H_4Ru_4(CO)_{10}[P(OMe)_3]_2$, 84254-45-5; $H_4Ru_4(CO)_9[P(OMe)_3]_3$, 34438-94-3; $H_4OS_4(CO)_{12}$, 12375-04-1; $H_4FeRu_3(CO)_{12}$, 11064-20-3; $H_2Ru_4(CO)_{13}$, 12110-32-6; $H_2FeRu_3(CO)_{13}$, 12375-24-5; $H_2Os_3(CO)_{12}$, 62863-43-8; $H_2Os(CO)_4$, 22372-70-9; $H_2Ru(CO)_4$, 42781-58-8; deuterium, 7782-39-0.

Crystal, Molecular, and Electronic Structures of Tetrasulfur Dinitride, S_4N_2

T. Chivers, P. W. Codding, W. G. Laidlaw, S. W. Liblong, R. T. Oakley,* and M. Trsic[1]

Contribution from the Department of Chemistry, University of Calgary, Calgary, Alberta, Canada T2N 1N4. *Received February 24, 1982*

Abstract: A simple method for obtaining high-purity S_4N_2 crystals is described. The crystal and molecular structure of S_4N_2 at −100 (5) °C has been determined by X-ray diffraction. Crystals of S_4N_2 are tetragonal, space group $P4_2nm$, $a = b = 11.146$ (4) Å, $c = 3.773$ (1) Å, $V = 468.7$ Å^3, and $Z = 4$. The refined structure ($R = 0.021$) shows the molecule to be a six-membered ring with the nitrogen atoms in the 1,3-positions. The molecule adopts a half-chair conformation with the central sulfur of the trisulfide unit lifted out of the plane of the remaining five atoms, producing a dihedral angle of 54.9°. Of the two types of S–N bonds, those linking the N–S–N moiety to the S_3 unit are considerably longer (1.676 (4) Å) than those within the N–S–N group (1.561 (4) Å). The S–S bonds (2.061 (2) Å) are as expected for an S–S single bond. MNDO and ab initio Hartree–Fock–Slater SCF calculations on a variety of model S_4N_2 structures show that the observed conformation is preferred by 6–10 kcal mol^{-1} (depending on the computational method) over a planar structure. The electronic structure and bonding are discussed on the basis of the HFS calculations on the crystal structure geometry and a related planar model. For the latter it is possible to assign 10 π-electron distributions formed by the weak interaction of two allyl-type fragments, S_3 and NSN. The strong visible absorptions observed for S_4N_2 (at 455 and 377 nm) are assigned to HOMO (π^*-type) → LUMO (π^*-type) and HOMO − 1 (π^*-type) → LUMO (π^*-type) excitations. The vibrational spectra of $S_4{}^{14}N_2$ and $S_4{}^{15}N_2$ are reported.

Of the known binary compounds of sulfur and nitrogen,[2] tetrasulfur dinitride, S_4N_2, has proven the most difficult to characterize structurally. Although the compound can be prepared by a variety of methods,[3] its low melting point (23 °C) and susceptibility to rapid thermal decomposition upon melting has made its manipulation an onerous task. The compound was first isolated in 1898 by Muthman and Clever, and their proposed formula, N_2S_5, serves to illustrate the susceptibility of the molecule toward disproportionation (hence their high sulfur content).[4] The correct composition "NS_2" was established in 1925,[5] but the molecular formula was not reported until 1951.[6] Twenty years later Nelson and Heal concluded, on the basis of mass, vibrational, and ^{14}N spectral data and dipole moment measurements that the most likely molecular structure was the six-membered ring **1**.[7]

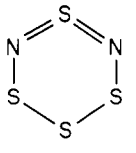

1

However, they could make no conclusive assignment regarding ring conformation. In 1972 Jolly pointed out that the most stable geometry should be one in which the central atom of the trisulfide sequence is tilted out of the plane of the remaining five atoms.[8] Subsequent CNDO/2 calculations by Adkins and Turner refuted this suggestion,[9] but more recent ab initio calculations have shown a preference for the nonplanar conformation.[10]

We have recently developed a simple method for preparing S_4N_2 and purifying it by crystallization from diethyl ether. The ready availability of this material has enabled us to determine its low-temperature crystal and molecular structure.[11] In order to probe the reasons for the observed solid state geometry, we have carried out ab initio Hartree–Fock–Slater (HFS) and MNDO molecular orbital calculations on a variety of model S_4N_2 structures. In addition we have examined in detail the nature of the electronic excitations responsible for the UV–visible absorptions of the molecule. The vibrational spectra of $S_4{}^{14}N_2$ and $S_4{}^{15}N_2$ in a variety of phases have also been measured, and these spectra are discussed in relation to the structure of the molecule.

Experimental Section

Preparation of S_4N_2. In a typical reaction, a solution of 25 mL of S_2Cl_2 in 75 mL of carbon disulfide was added dropwise (20 min) to a 1-L Erlenmeyer flask containing 200 mL of carbon disulfide and 200 mL of 12 M NH_4OH. During the course of the addition the reaction mixture

(1) Permanent address: Instituto de Física e Química de São Carlos, Universidade de São Paulo, 13560 São Carlos, S.P., Brazil.
(2) Chivers, T.; Oakley, R. T. *Top. Curr. Chem.* **1982**, *102*, 117.
(3) For examples, see: (a) Roesky, H. W. *Adv. Inorg. Radiochem.* **1979**, *22*, 239. (b) Heal, H. G. "The Inorganic Heterocyclic Chemistry of Sulfur, Nitrogen and Phosphorus"; Academic Press: London, 1980; p 115.
(4) Muthman, W.; Clever, E. *Z. Anorg. Allg. Chem.* **1897**, *13*, 200.
(5) Usher, F. L. *J. Chem. Soc.* **1925**, 730.
(6) Meuwsen, A. *Z. Anorg. Allg. Chem.* **1951**, *266*, 250.
(7) Nelson, J.; Heal, H. G. *J. Chem. Soc. A* **1971**, 136.
(8) Jolly, W. L. *Adv. Chem. Ser.* **1972**, *No. 110*, 92.
(9) Adkins, R. R.; Turner, A. G. *J. Am. Chem. Soc.* **1978**, *100*, 1383.
(10) Palmer, M. H.; Wheeler, J. R.; Findlay, R. H.; Westwood, N. P. C.; Lau, W. M. *J. Mol. Struct.* **1981**, *86*, 193.
(11) For a preliminary communication of part of this work, see: Chivers, T.; Codding, P. W.; Oakley, R. T. *J. Chem. Soc., Chem. Commun.* **1981**, 584.

0002-7863/83/1505-1186$01.50/0

Table I. Crystal Data

S_4N_2
cryst system: tetragonal
space group: $P4_2nm$
$M_r = 156.25$
$a = b = 11.146$ (4) Å
$c = 3.773$ (1) Å
$d_c = 2.21$ g cm^{-3}
$V = 468.7$ Å^3
$Z = 4$
radiatn: Mo Kα (graphite monochromator) $\lambda = 0.71069$ Å
max θ: 30.0°
scan type: ω–2θ
scan speed: 0.7–6.7° min^{-1} to give $I/\sigma(I) \geq 2.5$ to a maximum time/reflection of 120 s
scan range: $\Delta\omega = 1.5\ (0.50 + 0.347 \tan\theta)°$
standard reflctns: (0.0.2), (4.6.0), and (6.0.2) were remeasured every 1000 s of X-ray exposure time and showed no significant intensity fluctuation
temp: −100 (5) °C
reflctns: 914 reflctns were averaged to give 438 unique reflctns of which 295 had $I > 3\sigma(I)$
absorptn coeff: μ(Mo Kα) = 17.68 cm^{-1}
cryst dimensns: 0.1 × 0.2 × 0.2 mm

was stirred vigorously and cooled by immersing the flask in an ice–water bath. When the addition was complete the carbon disulfide phase was separated, washed with water, and dried over K_2CO_3. The solution was then concentrated on a rotary evaporator to ca. 50 mL and eluted through a short (100 × 25 mm) silica column. Solvent was removed from the eluant on a rotary evaporator to leave a dark red tar, from which S_4N_2 could be separated by slow sublimation (4–5 h) at room temperature and 10^{-2} torr onto a −78 °C (dry ice–acetone) cold finger. The crude material (generally 400–600 mg) was washed off the finger with CS_2 and subjected to a second sublimation in vacuo. This doubly sublimed material was then dissolved to the point of saturation in boiling diethyl ether. When this solution was cooled to −20 °C, lustrous dark red needles (mp 22.5–23.5 °C) separated and were removed by filtration at low temperature.

Crystal and Molecular Structure Determination. The crystal data and experimental conditions are given in Table I. A rectangular lath of S_4N_2 was mounted at 4 °C and placed under the cold N_2 stream of an Enraf-Nonius LT-1 low-temperature device on a CAD 4F automated diffractometer. The computer indexing routine identified the unit cell as tetragonal; this cell assignment and the space group were confirmed by the examination of the intensities from a data collection ($2° < \theta \leq 10°$) over the entire sphere of reflection. The cell constants and the orientation matrix were determined by least-squares refinement of the diffraction geometry for 25 reflections with $8.5° \leq \theta \leq 15.7°$. An ω–2θ scan was used for the data collection; the scan was collected in 96 steps, of which the first and last 16 steps were considered as background. Intensities were calculated as $I = [P - 2(B1 + B2)]Q$, where P is the sum of the central 64 steps, Q is the scan rate, and $B1$ and $B2$ are the background counts. The standard deviation of the intensity is $\sigma(I) = [P + 4(B1 + B2)]^{1/2}Q$. Lorentz and polarization corrections were applied and E values were calculated by using a K curve.

Initial coordinates for the four atoms in the asymmetric unit (the molecule is positioned on a mirror plane which contains two of the sulfur atoms) were obtained with MULTAN 78.[12] Isotropic and anisotropic refinements, using unit weights, resulted in a final agreement factor of $R = 0.021$. On the final cycle the maximum shift/error was 0.004, and the standard deviation of an observation of unit weight was 2.08.

Spectroscopic Measurements. The UV–visible spectrum of S_4N_2 (in hexane solution) was recorded on a Cary 219 spectrophotometer, utilizing the automatic base-line mode. Infrared spectra (on Nujol mulls and in CS_2 solution with CsI cells) were recorded on a Perkin-Elmer 580 spectrophotometer. $S_4{}^{15}N_2$ was prepared as previously described.[14] Raman spectra were recorded on samples in a variety of phases with a Jarrel-Ash Model 25-100 double-grating spectrophotometer with a photon counting detection system and a Coherent Radiation CR-4 argon ion laser. Although attempts were made to obtain spectra in the solid state (with a 6-cm diameter ring spinning at 1000 rpm) and in the liquid phase (with a small spinning bulb), useful spectra could only be obtained on samples in CS_2 solution (in glass capillaries). Even then resolution was extremely poor, and sample decomposition occurred within 15 min in the laser beam (cf. ref 7).

Table II

atom	x/a	y/b	z/c
(1) Fractional Atomic Coordinates (×10^5) for S_4N_2			
S(1)	38 869 (9)	38 869[a]	56 294[b]
S(2)	−17 863 (9)	−17 863[a]	50 813 (71)
S(3)	14 505 (9)	34 959 (9)	32 515 (64)
N	25 685 (30)	43 082 (31)	49 983 (133)

(2) Bond Distances (Å) and Bond Angles (deg) for S_4N_2

S(1)–N	1.561 (4)
S(2)–S(3)	2.061 (2)
S(3)–N	1.676 (4)
N–S(1)–N′	122.9 (2)
S(3)–S(2)–S(3′)	102.92 (9)
S(2)–S(3)–N	103.4 (2)
S(1)–N–S(3)	126.7 (2)

[a] Fixed by symmetry. [b] Fixed to define the origin along the c axis.

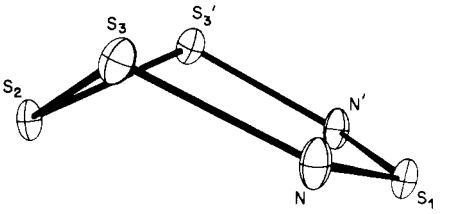

Figure 1. ORTEP drawing of S_4N_2 showing the atomic numbering scheme.

Theoretical Calculations. The MNDO program used was developed by Dewar and co-workers[15] and has been shown to provide adequate orbital energies on a variety on sulfur–nitrogen molecules.[16] The SCF-HFS procedure as implemented by Baerends and co-workers[17] was used, keeping the core orbitals "frozen" during the iterations. In the HFS case the double ζ basis set described by Clementi and Roetti[18] was augmented with a 3d function on sulfur.[19] For electronic transition energies a spin-unrestricted version of the HFS method and the transition state approximation were utilized.[20]

Results and Discussion

Preparation and Purificatoin of S_4N_2. Many methods have been reported for preparing S_4N_2. In our work we have developed a useful modification of the procedure originally described by Niinistö and Laitenen.[21] As described herein the reaction of sulfur monochloride and aqueous ammonia provides a fast and relatively easy route to half-gram quantities of the compound. However, of more importance than the preparative method itself is the procedure used for the purification of the compound. Crystals of S_4N_2 purified by crystallization from diethyl ether (see Experimental Section) show no tendency to decompose in the solid state. We have kept such crystals at −20 °C in an unsealed vial with absolutely no change in their physical appearance or infrared spectrum for periods in excess of 1 year. However, crystalline samples of S_4N_2 purified by sublimation alone do decompose slowly on standing, even in vacuo at −20 °C. This change is *not*, we believe, the result of a spontaneous decomposition of S_4N_2 itself to yield $(SN)_x$, as has been proposed recently.[22] Instead, we

(12) All other programs used were part of the XRAY-76 system of programs implemented on a Honeywell Multics operating system by Judith A. Konnert of the U.S. Geological Survey and P. W. Codding. Atomic scattering factors were those of Cromer and Mann (ref 13).

(13) Cromer, D. T.; Mann, J. B. *Acta Crystallogr., Sect. A* **1968**, *A24*, 321.

(14) Chivers, T.; Oakley, R. T.; Scherer, O. J.; Wolmershaüser, G. *Inorg. Chem.* **1981**, *20*, 914.

(15) Dewar, M. J. S.; Thiel, W. *J. Am. Chem .Soc.* **1977**, *99*, 4399.

(16) (a) Gleiter, R.; Bartetzko, R. *Z. Naturforsch. B: Anorg. Chem., Org. Chem.* **1981**, *36B*, 492. (b) Sensarma, S.; Turner, A. G. *Inorg. Chim. Acta* **1982**, *64*, L161.

(17) (a) Baerends, E. J.; Ellis, D. E.; Ros, P. *Chem. Phys.* **1973**, *2*, 41. (b) Baerends, E. J.; Ros, P. *Int. J. Quantum Chem. Symp.* **1978**, *12*, 169.

(18) Clementi, E.; Roetti, C. *At. Data Nucl. Data Tables.* **1974**, *14*, 177.

(19) Exponent $Z = 1.68$. This is an optimal value. See: Reference 31.

(20) Ziegler, T.; Rauk, A.; Baerends, E. J. *Theor. Chim. Acta* **1977**, *43*, 261.

(21) Niinistö, L.; Laitenen, R. *Inorg. Nucl. Chem. Lett.* **1976**, *12*, 191.

(22) Small, R. W.; Banister, A. J.; Hauptman, Z. V. *J. Chem. Soc., Dalton Trans.* **1981**, 2188.

Table III. Geometrical Parameters,[a] Calculated HFS Charges, and Total Atom-Atom Overlap Populations for S_4N_2 (Models I and II)

A. Geometrical Parameters

	$d(S_a\text{-}N)$	$d(S_b\text{-}N)$	$d(S\text{-}S)$	$\angle S_a$	$\angle S_c$	θ[b]
I	1.56	1.68	2.06	122.9	102.8	54.9
II	1.56	1.68	2.06	122.9	102.8	0

B. Calculated HFS Charges

	S_a	N	S_b	S_c
I	0.52	−0.36	0.12	−0.04
II	0.39	−0.33	0.13	0.02

C. Overlap Populations

	$S_s\text{-}N$	$S_b\text{-}N$	S-S
I	0.63	0.43	0.46
II	0.58	0.49	0.40

[a] Distances in Å, angles in degrees. See 4 for atom labeling scheme. [b] θ is the dihedral angle between the $S_b\text{-}S_c\text{-}S_b$ and $S_b\text{-}N\text{-}S_a\text{-}N\text{-}S_b$ planes.

suggest that trace impurities of S_2N_2, which are coproduced in many of the synthetic routes to S_4N_2, catalyze its polymerization to $(SN)_x$. Such processes are not without precedent. The reaction of S_4N_4 with bromine vapors to produce brominated $(SNBr_{0.4})_x$ polymer is well-known.[23] We are currently exploring the reactivity of fully purified S_4N_2 crystals with a variety of oxidizing media (e.g., bromine vapors, ICl, NOCl, SbF_5).

Molecular Structure. The atomic coordinates, bond distances, and bond angles for S_4N_2 are given in Table II. The molecular structure, as shown in Figure 1, is a six-membered ring with nitrogen atoms occupying the 1,3-positions. The ring is nonplanar and the angle between the two planar moieties S(3′)–S(2)–S(3) and S(3)–N–S(1)–N′–S(3′), σ(plane) = 0.03 Å, is 54.9°. Subsequent to our communication of this structure,[11] which was determined at −100 °C, another determination at a higher temperature (5 °C) was reported.[22] The ring conformation and bond lengths and angles in the two determinations are similar although trends are more pronounced in the more precise low-temperature version described here (R = 0.021 vs. R = 0.050[22]).

Of the bond distances and angles in this structure, the S–N distances are most noteworthy. The S(3)–N distance of 1.676 (4) Å is appreciably longer than the S(1)–N bond (1.561 (4) Å). The two values approach those expected for S–N single (1.73 Å)[24] and double (1.57 Å)[24] bonds, respectively. In the planar $S_3N_3^-$ anion, the approximately equal S–N bond lengths of 1.61 Å are intermediate between the two lengths found for S_4N_2. The bond angle subtended by the nitrogen atom in S_4N_2 is larger by more than 3° than the average S–N–S angle in $S_3N_3^-$ (127.7 (2)° vs. 123.2[25]), even though the local environment of the nitrogen atom in each ring is approximately planar. Also the angle at S(1) is ca. 6° larger than the average N–S–N angle in $S_3N_3^-$, 122.9 (2)° and 116.6°, respectively. These wider angles are probably due to the distortion of the ring from C_3 symmetry (present in $S_3N_3^-$) occasioned by the longer skeletal bonds of the S–S–S unit. The S–S distance of 2.061 (2) Å and the S(3)–S(2)–S(3′) angle of 102.92 (9)° are similar to those observed in S_6, 2.06 Å and 102°, respectively.[26]

Electronic Structure. In contrast to the many molecular orbital studies on tetrasulfur tetranitride, S_4N_4,[27,33] and disulfur dinitride, S_2N_2,[27] relatively few reports have appeared discussing the electronic structure of S_4N_2. In their CNDO/2 study Adkins and Turner[9] assumed a molecular structure which, although reasonable at the time, differs significantly from that determined by X-ray diffraction (see previous section). Very recently Palmer et al.[10] published a preliminary note outlining the results of an ab initio calculation with full geometry optimization which yields a predicted structure that agrees remarkably with the crystal structure geometry we report herein. Although some comments on the energy levels reported by these latter authors will be made in the course of our discussion, it seems inappropriate to undertake a detailed analysis of their preliminary results at this time.

Our own interest in the electronic structure of S_4N_2 stems in part from our recent studies on two related six-membered ring systems; $S_3N_3^-$ (**2**)[24] and $H_2PS_2N_3$ (**3**).[28] The former can be

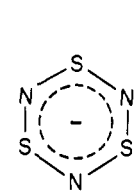

2

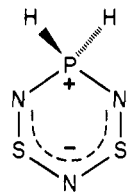

3

considered as a fully delocalized 10 π-electron 6-atom perimeter, while the latter has a more pentadienyl-like structure, with 8 π electrons distributed primarily over the 5-atom NSNSN sequence. On the basis of these concepts, many physical (e.g., electronic[25,28] and MCD spectra[29]) and chemical properties (e.g., ease of oxidation[30] and cycloaddition chemistry[28]) are readily understood. While S_4N_2 is not planar and a rigorous separation of π and σ systems not possible, it is tempting to develop a delocalized description similar to those found in **2** and **3** by considering its electronic structure in terms of the expected perturbations on the MO manifold of $S_3N_3^-$. Although intuitively reasonable, such an approach fails to explain in simple terms a most important feature of the crystal structure geometry, namely the long central N–S bonds. Furthermore, it is unable to account for the known tendency of the molecule to thermally decompose to elemental sulfur and dinitrogen. The reasons for the low activation energy for this process have not hitherto been addressed, but in our original communication on the structure of S_4N_2 we suggested that the long central N–S links indicated a possible mechanism for disproportionation, i.e., via the rupture of these bonds to produce S_3[31] and NSN[32] fragments. We have, therefore, chosen to analyze the electronic structure of S_4N_2 with this possibility in mind.

Our strategy in the present work has been to carry out both semiempirical MNDO and ab initio Hartree–Fock–Slater calculations on several molecular geometries, focusing principally on the two models defined in Table III (see also **4**). Model I replicates the geometry observed in the solid state (at −100 °C) while model II represents a planar version of I. In the following paragraphs we show how the π structure of a planar S_4N_2 molecule (II) can be considered as a union of the two molecular fragments S_3 and NSN. The observed half-chair conformation of the

(23) (a) Bernard, C.; Herold, A.; Telaurin, M.; Robert, G. *C. R. Hebd. Seances Acad. Sci. Ser. C.* **1976**, *283*, 625. (b) Street, G. B.; Gill, W. D.; Geiss, R. H.; Greene, R. L.; Mayerle, J. J. *J. Chem. Soc., Chem. Commun.* **1977**, 407. (c) Akhtar, M.; Kleppinger, J.; Macdiarmid, A. G.; Milliken, J.; Moran, M. J.; Chiang, K.; Cohen, M. J.; Heeger, A. J.; Peebles, D. L. *Ibid.* **1977**, 473.

(24) (a) Cruickshank, D. W. J. *J. Chem. Soc.* **1961**, 5486. (b) Chapman, D.; Waddington, T. C. *Trans. Faraday Soc.* **1962**, *58*, 1679. (c) Nyburg, S. C. *J. Cryst. Mol. Struct.* **1973**, *3*, 331.

(25) (a) Bojes, J.; Chivers, T.; Laidlaw, W. G.; Trsic, M. *J. Am. Chem. Soc.* **1979**, *101*, 4517. (b) Chivers, T.; Laidlaw, W. G.; Oakley, R. T.; Trsic, M. *Inorg. Chim. Acta* **1981**, L189.

(26) Donohue, J.; Caron, A.; Goldish, E. *J. Am. Chem. Soc.* **1961**, *83*, 3948.

(27) See, for example: (a) Findlay, R. H.; Palmer, M. H.; Downs, A. J.; Egdell, R. G.; Evans, R. *Inorg. Chem.* **1980**, *15*, 1307. (b) Haddon, R. C.; Wasserman, S. R.; Wudl, F.; Williams, G. R. J. *J. Am. Chem. Soc.* **1980**, *102*, 6687 and references therein.

(28) Burford, N.; Chivers, T.; Cordes, A. W.; Laidlaw, W. G.; Noble, M. C.; Oakley, R. T.; Swepston, P. N. *J. Am. Chem. Soc.* **1982**, *104*, 1282.

(29) Waluk, J. W.; Michl, J. *Inorg. Chem.* **1981**, *20*, 563.

(30) Chivers, T.; Oakley, R. T.; Cordes, A. W.; Pennington, W. T. *J. Chem. Soc., Chem. Commun.* **1981**, 1214.

(31) The 4-π-electron configuration $a_1^2a_2^2b_1^2b_2^0$ of S_3 is used for comparison. See: Laidlaw, W. G.; Trsic, M. *Chem. Phys.* **1979**, *36*, 323.

(32) The 4-π-electron configuration $a_1^2a_2^2b_1^2b_2^0$ of NSN is used for comparison. See: Laidlaw, W. G.; Trsic, M. *Inorg. Chem.* **1981**, *20*, 1792.

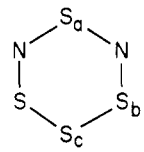

4

molecule can then be understood in terms of a reorganization of the σ and π systems so as to produce a (marginally) more stable entity.

Molecular Orbital Description. Table IV shows the ab initio HFS orbital energies and overlap populations obtained for the S_4N_2 molecule with the solid-state structural parameters (I). The total overlap population for N–S_b (0.43) indicates a slightly weakened N–S single bond, whereas the N–S_a bonds (0.63) appear to be considerably stronger. The overlap population of the S_b–S_c bond (0.46) is approximately that of a single bond. The calculated charges imply a polarized N–S_b bond (q_N = –0.36, q_S = 0.12); and a highly polarized N–S_a bond (q_N = –0.36, q_S = 0.52), indeed the latter is more polarized than in the isolated NSN fragment (with ∠S = 120°, d(S–N) = 1.62 Å, q_N = –0.17, q_S = 0.35), and is comparable to the NS bonds in the $S_4N_5^+$ cation.[33] Figure 2 illustrates the orbital energy sequence for the upper levels of the stack for model I along with the corresponding levels for model II.[34] As predicted by Banister,[35] and in agreement with the early CNDO/2 results of Adkins and Turner,[9] the planar model has five occupied orbitals of π symmetry ($1b_1$, $1a_2$, $2b_1$, $2a_2$ and $3b_1$). There is, in addition, a low lying empty π orbital $4b_1$. Analysis of the eigenvectors of the LUMO (11a′), the HOMO (7a″), and HOMO – 1 (10a′) of model I shows them to be primarily π-type orbitals.[36] The approximate correlation of these orbitals to the strictly π MO's $4b_1$, $2a_2$, and $3b_1$ (illustrated in Figure 2) is easy to establish. As one moves further down the energy level stack the correlation from S_4N_2 (I) to S_4N_2 (II) becomes less clear-cut. When the π symmetry is broken, there is considerable mixing of $1a_2$ and $4b_2$, and also of $2b_1$ and $7a_1$, with the result that the π character of $1a_2$ and $2b_1$ is distributed over several orbitals ($1a_2$ → 4a″ and 5a″, and $2b_1$ → 8a′ and 9a′). However, the lowest π orbital $1b_1$ retains its integrity as a π-like orbital 6a′.

Although the above correlation of orbitals for S_4N_2 (I and II) is less than perfect, it provides a basis for describing the bonding changes which occur on passing from the nonplanar to the planar conformation. In order to understand the bonding in both models, it is useful to begin by examining the π system of the latter model (II). The overlap populations for the occupied π orbitals and the LUMO of the π manifold of S_4N_2 (II) are given in Table V. It is evident that the lowest π orbital, $1b_1$, is strongly bonding in the N–S_a–N moiety, $1a_2$ is strongly bonding in the N–S_b bonds and $2b_1$ is strongly bonding in the S_3 unit. The $2a_2$ orbital is antibonding in the N–S_b bonds, while the uppermost orbitals $3b_1$ and $4b_1$ are antibonding primarily in the S_3 and NSN regions, respectively. Such a pattern is precisely what one would expect for two allyl-type fragments interacting principally through their a_2 orbitals. This point is illustrated in Figure 3, which provides a HFS energy level diagram for the π MO's of the two three-atom fragments S_3[31] and NSN[32] along with those of S_4N_2 (II). As can be seen the a_2 levels of the two fragments are very close in energy, so that a strong interaction is to be expected; consequently, the two a_2 levels of S_4N_2 (II) are widely separated. The two bonding levels $1b_1$ and $2b_1$ of S_4N_2 remain largely unchanged in composition and energy from their parent orbitals in S_3 and NSN. Likewise the two antibonding orbitals $3b_1$ and $4b_1$ of S_4N_2 (II) retain much of the character of the two $2b_1$ orbitals of S_3 and NSN. Since both the bonding and antibonding orbitals associated with the S_3 fragment are occupied, there should be a net "cancellation" resulting in no net π bonding in the S_3 portion of the molecule. However, since the antibonding orbital $4b_1$, located on the NSN fragment, is not occupied, a residual π bond would

Table IV. Energies and Atom–Atom Overlap Populations (Mulliken Populations) for the MO's of S_4N_2 (Model I) from the HFS Calculation (C_s Symmetry)

orbitals	atom–atom overlap populations S_b–S_c	S_b–N	S_a–N	eigenvalues (–, au)
1a′	0.003	0.022	0.066	0.9161
2a′	0.061	0.005	0.017	0.8686
3a′	0.002	0.055	–0.009	0.6383
4a′	–0.032	–0.037	–0.030	0.4505
5a′	0.002	0.020	0.017	0.3982
6a′	–0.003	0.013	0.044	0.3904
7a′	0.023	–0.010	–0.004	0.3180
8a′	0.024	–0.028	–0.033	0.3070
9a′	–0.001	–0.003	–0.010	0.2690
10a′	–0.032	0.009	–0.010	0.2096
11a′ (LUMO)	–0.041	–0.007	–0.084	0.1058
1a″	0.002	0.055	0.028	0.8275
2a″	0.024	–0.012	0.040	0.6509
3a″	0.042	0.027	0.013	0.4860
4a″	0.001	0.011	0.004	0.3480
5a″	0.000	0.041	0.011	0.3043
6a″	–0.011	–0.012	0.006	0.2564
7a″ (HOMO)	0.008	–0.048	0.009	0.1818

Table V. Atom–Atom Overlap Populations for the π MO's of S_4N_2 (Model II) from the HFS Calculation (C_{2v} Symmetry)

orbital	atom–atom overlap population S_b–S_c	S_b–N	S_a–N
$1b_1$	0.006	0.019	0.044
$2b_1$	0.049	–0.008	0.011
$3b_1$ (HOMO)	–0.050	0.019	–0.022
$1a_2$	0.002	0.043	0.013
$2a_2$	0.010	–0.043	0.018
total (×4)	0.07	0.12	0.27
$4b_1$ (LUMO + 2)	–0.029	–0.032	–0.083

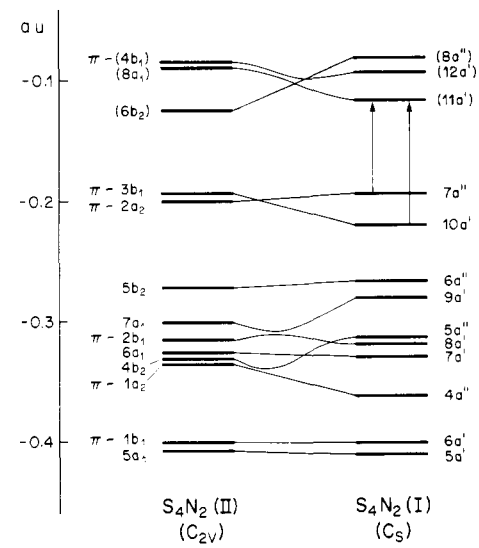

Figure 2. Correlation diagram for the HFS energy levels of S_4N_2 in the nonplanar conformation I and the planar conformation II (only the upper levels of the stack are shown). The two low-energy electronic transitions of S_4N_2 (I) are indicated with vertical arrows. Unoccupied levels are indicated by parentheses.

(33) Chivers, T.; Fielding, L.; Laidlaw, W. G.; Trsic, M. *Inorg. Chem.* **1980**, *18*, 3379.

(34) The ordering for the upper part of the stack of S_4N_2 (model I) is very similar to that reported in ref 10. However, in the case of model II there is a reversal of several of the levels from those described by Palmer et al. for their planar model.

(35) Banister, A. J. *Nature (London), Phys. Sci.* **1972**, *237*, 92.

(36) Correlation of the two models is facilitated by designating those orbitals in I which are "π-like". By this we mean those which are antisymmetric with respect to the local molecular plane at a given atom. Even so several avoided crossings prevent a one-to-one correlation of all the orbitals of I and II.

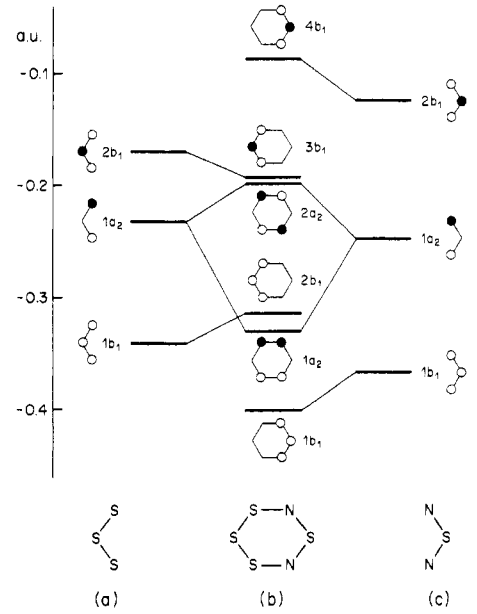

Figure 3. Correlation diagram for the π orbitals of S_3 (a), NSN (c), and S_4N_2 II (b). For the S_3 and NSN fragments the energy levels correspond to the geometry of the units as they are found in S_4N_2.

be expected for this portion of the molecule. The occupancy of both the $1a_2$ and $2a_2$ orbitals of S_4N_2 also effects a "cancellation" of bonding and antibonding contributions, in this instance for the N–S_b linkages. The calculated net π populations (N–S_a, 0.26; N–S_b, 0.12; S_b–S_c, 0.07) certainly provide a qualitative confirmation of this simple picture.[37] The correspondence is not ideal because some delocalization of the orbitals of the two islands (S_3 and NSN) over the entire six-atom perimeter is observed in all the MO's of S_4N_2 (II) (see Table V). However its extent is limited, far more so than in $S_3N_3^-$ (**2**) or in $H_2PS_2N_3$ (**3**).

This characterization of the π system of the planar model is a useful starting point for discussing the nature of the electronic structure of the solid-state geometry (I). Certainly the breaking of the six-center plane of symmetry caused by lifting S_c out of the plane will affect the p_π overlap in the S_b–S_c and N–S_b bonds, but it should have less effect on the NSN unit. Examination of the orbitals to which the π system evolves shows that "cancellation" of the antibonding and bonding character is maintained in the S_3 portion of S_4N_2 and that indeed the π bond in the N–S_a–N region persists. Furthermore, the added flexibility occasioned by the lowered symmetry allows rearrangement of the σ framework and the enhancement of the total overlap populations for the S_b–S_c (from 0.40 to 0.46) and N–S_a (from 0.58 to 0.63) bonds. However, breaking the π plane of symmetry destroys the approximate "cancellation" of the π-bonding contributions in the N–S_b linkage. Indeed this contribution goes from weakly bonding (0.12 overlap population) to antibonding. What is perhaps of more importance is the fact that this decrease in N–S_b overlap in the π-type orbitals is not compensated by a strengthening of the N–S_b σ bond. As a result the N–S_b link is weakened (the total overlap population drops from 0.49 to 0.43)—in contrast to the strengthened N–S_a and S_b–S_c bonds. The consequent integrity of the S_3 and NSN fragments and the susceptibility of S_4N_2 to decomposition via

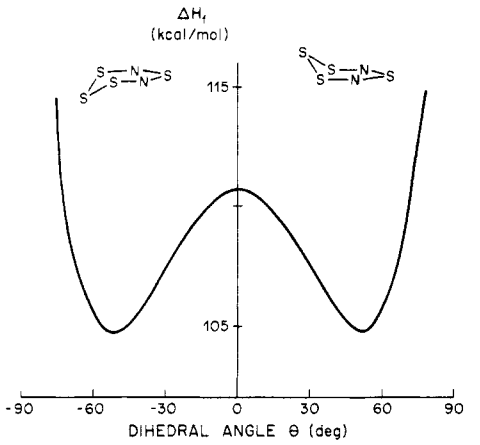

Figure 4. Calculated (MNDO) heat of formation (ΔH_f) of S_4N_2 as a function of θ, the dihedral angle between the S_3 and SNSNS planes. Apart from the restriction on the value of θ and the planarity of the SNSNS fragment, the calculations were performed with full geometry optimization.

cleavage of the N–S_b bonds does not, therefore, seem unreasonable.

Conformational Analysis of S_4N_2. As was pointed out in the previous section, the principal difference between the bonding in the planar and nonplanar conformations of S_4N_2 is the weakening of the π bonding for N–S_b and the enhancement of the σ network in the S_3 and NSN regions. Total energy calculations using the HFS method indicate the rearrangement from II to I to be favorable, by about 10 kcal mol^{-1}. At the MNDO level the calculated energy difference is comparable (11 kcal mol^{-1} in favor of I). Full geometry optimization with MNDO performed on a series of conformations differing only in their dihedral angles θ predicts that the global energy minimum, as a function of θ, lies remarkably close (at $\theta = 52 \pm 2°$) to the actual solid-state geometry value of 54.9° (see Figure 6). Full optimization also lowers the half-chair/half-chair inversion barrier to near 6 kcal mol^{-1}. The calculations by Palmer et al.[10] indicate the same region for the energy minimum but suggest a slightly higher inversion barrier (ca. 14 kcal mol^{-1}). Although these numerical differences should not be given too great significance, we would expect the barrier to be smaller than in 1,2,3-trithiane (**5**) (observed value 13.2 kcal

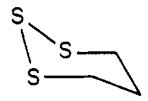

5

mol^{-1},[39] calculated value 12.3 kcal mol^{-1} [40]), where conjugative effects in the transition state would be absent.

Although these energy differences are near the limit of reliability of the calculation, it is apparent that the energy balance between models II and I of S_4N_2 favors the latter. The reorganization of the S_3 fragment and at S_a in the N–S_a–N unit is therefore more crucial than the loss of the N–S_b π bond. In S_6, where the appropriate orientation of nonbonding distributions is even more crucial, a full chair conformation, with an inversion barrier of 29.9 kcal mol^{-1},[40] is observed. However, in $S_3N_3^-$ this reorganization is less important (in view of the greater charge carrying capacity of nitrogen), and a planar structure is observed.[24a]

Electronic Spectrum of S_4N_2. The UV–visible spectrum of S_4N_2 in hexane solution (Figure 5) contains two low-energy absorptions with λ_{max} values at 455 and 377 nm. In addition a higher energy band, which may contain more than one component, is observed at 232 nm. In order to probe the nature of these electronic

(37) We view the S_4N_2 molecule (model II) as a 10π system (there are 5 occupied π MO's). If the idealized "cancellation" process described herein is carried to its logical conclusion, there is a net π-bonding contribution from 2 π electrons, localized primarily over the N–S_a–N fragment. Bhattacharyya et al. (ref 38) have recently stressed the importance of such an approach to π bonding. Their results on S_4N_2 suggest a total of 4 π electrons on the N–S_a–N moiety. However, while a discussion of the net π bonding has some merit in regard to bond order considerations, its limitations must be recognized. The frontier orbitals are the π^*-MO's, and their influence on chemical reactivity and physical properties (e.g., electronic and MCD spectra) cannot be canceled out.

(38) Bhattacharyya, A. A.; Bhattacharyya, A.; Adkins, R. R.; Turner, A. G. *J. Am. Chem. Soc.* **1981**, *103*, 7458.

(39) Kabuss, S.; Luttringhaus, A.; Friebolin, H.; Mecke, R. *Z. Naturforsch. B: Anorg. Chem., Org. Chem.* **1966**, *21B*, 320.

(40) Allinger, N. L.; Hickey, M. J.; Kao, J. *J. Am. Chem. Soc.* **1976**, *98*, 2741.

Table VI. Vibrational Spectra of $S_4{}^{14}N_2$ and $S_4{}^{15}N_2$[a]

infrared (Nujol mull)	Δ[b]	infrared (liquid film)	Δ[b]	infrared (CS_2 solution)	Δ[b]	Raman (CS_2 solution)	Δ[b]
1034 (1018) (s)	16	1034 (1013) (s)	21	1033 (1012) (s)	21		
918 (893) (w)	25	929 (905) (w)	24	929 (905) (w)	24	929 (902) 10, p	27
635 (623) (s)	12	630 (620) (vs)	10	629 (619) (s)	10	624 (624) 2, dp	0
628 (609) (vs)	19	621 (601) (s)	20	620 (601) (s)	19		
561 (560) (m)	1						
469 (468) (m)	1	469 (468) (m)	1	470 (469) (w)	1	468 (469) 3, p	−1
376 (368) (ms)	8	374 (368) (m)	6	377 (368) (m)	9	378 (372) 1, ?	6
322 (316) (m)	6	321 (314) (m)	7	320 (313) (w)	7		
266 (265) (vw)	1	266 (265) (vw)	1	266 (265) (vw)	1	264 (264) 1, ?	0

[a] In cm^{-1}. Numbers in parentheses refer to $S_4{}^{15}N_2$. [b] The isotopic shift $\Delta = \nu(S_4{}^{14}N_2) - \nu(S_4{}^{15}N_2)$, in cm^{-1}.

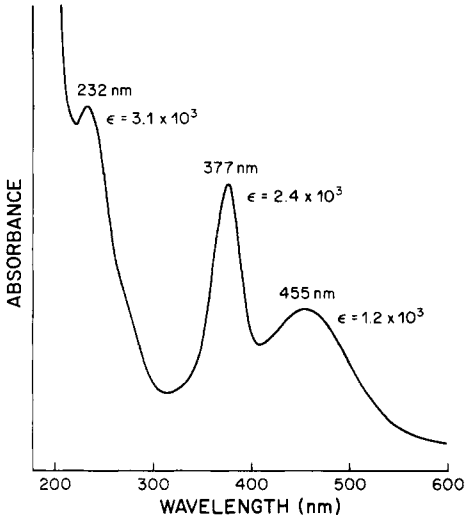

Figure 5. UV–visible spectrum of S_4N_2 (in *n*-hexane).

transitions, we have calculated the oscillator strengths for all transitions from the three highest occupied orbitals to the three lowest unoccupied levels (all of which are symmetry allowed).[41] The most probable transitions are 7a″ → 11a′, 10a′ → 11a′, 6a″ → 11a′, and 6a″ → 8a″; these have relative strengths (calculated) of 3:2:1:1. Using the transition-state method,[19] we have calculated the energies of these transitions as 500, 392, 270, and 220 nm. Consequently, we assign the 455-nm band in S_4N_2 to the 7a″ → 11a′ (HOMO → LUMO) excitation and the 377-nm band to the 10a′ → 11a′ (HOMO − 1 → LUMO) excitation. Although the observed extinction coefficients of these bands do not match the calculated oscillator strengths particularly well, integration provides experimental oscillator strengths in the ratio of 1.2:1 for the 455- and 377-nm bands, which is in reasonable agreement with the 1.5:1 calculated ratio. The band at 232 nm would likely be dominated by the 6a″ → 8a″ excitation but would also contain contributions from the 6a″ → 11a′ transition (among others).

On the basis of our earlier analysis of the character of the orbitals involved in the two low-energy transitions, we propose that they may be viewed as π^*-type → π^*-type excitations. As we have stated, delocalization over the entire ring is limited, but to the extent that it survives, its presence is most apparent in the upper levels, i.e., 7a″, 10a′, and 11a′. Confirmation of our assignment through the analysis of the MCD spectrum of S_4N_2 (treated as a 10-π-electron 6-atom perimeter) should be possible.

Vibrational Spectra of S_4N_2. The molecular orbital calculations described in the previous section suggest that the energetically preferred conformation of S_4N_2 is a half-chair structure similar to that observed in the solid state. Although the calculated inversion barrier is not necessarily an accurate value, its magnitude (~6–10 kcal mol^{-1}) suggests that the inversion process would not be observable with vibrational spectroscopy. The rate of inversion is much slower than the time scale of the experiment. Nonetheless, we do observe some interesting changes in the infrared spectrum of S_4N_2 upon passing from the solid state to liquid and solution samples. Table VI gives the frequencies of the infrared and Raman bands of $S_4{}^{14}N_2$ and $S_4{}^{15}N_2$, as obtained under a variety of conditions. The poor resolution of the Raman spectrum of S_4N_2 prevents its detailed analysis, but in the infrared region >250 cm^{-1} a total of nine bands are observed in the solid-state (Nujol mull) spectrum (Figure 6a). However, when S_4N_2 is melted or dissolved in CS_2 (or CCl_4), one of these bands (at 561 cm^{-1}) is lost and several others (at 918, 630, and 628 cm^{-1}) undergo significant

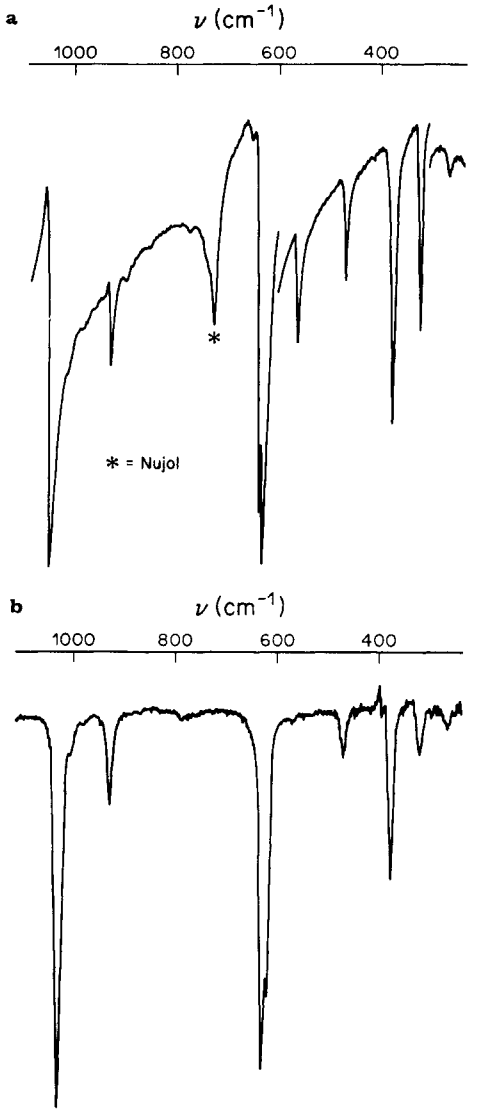

Figure 6. Infrared spectrum (1200–250-cm^{-1} region) of S_4N_2 as obtained from (a) a Nujol mull (at 0 °C) and (b) a CS_2 solution (solvent bands have been subtracted).

(41) The dipole length–dipole velocity formula for the oscillator strength was employed. See: Trsic, M.; Zeigler, T.; Laidlaw, W. G. *Chem. Phys.* **1976**, *15*, 323.

(42) Weiser, H.; Krueger, P. J.; Muller, E.; Hyne, J. B. *Can. J. Chem.* **1969**, *47*, 1633.

shifts and/or intensity alterations (Figure 6b and Table VI).

In C_s symmetry all 12 fundamental vibrational modes of S_4N_2 are expected to be infrared active, but in C_{2v} (planar) symmetry one vibration (an out-of-plane ring deformation A_2) will become inactive. It is therefore interesting to speculate whether the disappearance of the 561-cm^{-1} band in liquid and dissolved samples represents a net increase in symmetry of S_4N_2. However, isotopic substitution with ^{15}N indicates virtually no isotope shift for the 561- and 469-cm^{-1} bands, suggesting that they are the ν_{asym} and ν_{sym} modes of the S-S-S group. In H_2S_3 these vibrations are observed at 477 and 487 cm^{-1}.[42] Thus, if the 561-cm^{-1} band is the ν_{asym}(S-S-S) stretching mode, its disappearance on phase change is hard to explain, since, regardless of any symmetry change, it should remain infrared active. The resolution of the problem is beyond the scope of the present study. As Table VI indicates, the number of vibrations which undergo isotope shifts indicates that S_4N_2 is a strongly coupled system and not amenable to an elementary vibrational analysis.

Summary

The X-ray crystal structure determination of S_4N_2 has established that the molecule is a nonplanar ring, with the central sulfur of the trisulfide sequence lifted out of the plane of the remaining five atoms. The calculated barrier for the half-chair/half-chair inversion is approximately 6-10 kcal mol^{-1}. On the basis of ab initio HFS molecular orbital calculations, the electronic structure of planar S_4N_2 can be satisfactorily rationalized in terms of interacting S_3 and NSN fragments. Although there is significant *net* π bonding in the NSN moiety, there is essentially no *net* π bonding for the remaining N-S and S-S links. In the half-chair conformation the σ system in the S_3 and NSN fragments is strengthened at the expense of weakened central N-S bonds, the net effect favoring the nonplanar geometry. The electronic spectrum of S_4N_2 exhibits two strong low-energy transitions which we assign to HOMO (π^*-type) → LUMO (π^*-type), and HOMO - 1 (π^*-type) → LUMO (π^*-type) transitions.

Acknowledgment. We thank the Natural Sciences and Engineering Research Council of Canada and FINEP of Brazil for financial support and for an NSERC University Research Fellowship (to R.T.O.). We are grateful to Kim Wagstaff for his assistance in obtaining the MNDO and HFS results.

Registry No. S_4N_2, 32607-15-1; S_2Cl_2, 10025-67-9; NH_4OH, 1336-21-6; ^{15}N, 14390-96-6.

Supplementary Material Available: A listing of structure factor amplitudes and a table of anisotropic thermal parameters for S_4N_2 (3 pages). Ordering information is given on any masthead page.

Crystal Structure of Dehydrated Ca-Exchanged Zeolite A. Absence of Near-Zero-Coordinate Ca^{2+}. Presence of Al Complex

Joseph J. Pluth and Joseph V. Smith*

Contribution from the Department of the Geophysical Sciences, The University of Chicago, Chicago, Illinois 60637. *Received April 19, 1982*

Abstract: After various exchange procedures were tested, crystals of Linde zeolite 4A were exchanged with 1 M $CaCl_2$ solution at room temperature for 6 days. Electron microprobe analysis gave $Na_{0.4}Ca_{5.2}Al_{11.5}Si_{12.5}O_{48}\cdot xH_2O$ with a possible trace of K and Mg. X-ray diffraction data for a crystal dehydrated at 350 °C were refined in space group $Fm\bar{3}c$ (a = 24.44 Å). Because of weakness of diffraction intensities, the mean T-O distances (1.58 and 1.73 Å) have low precision but are consistent with the earlier evidence for alternation of tetrahedra populated by Si and $\sim Al_{0.9}Si_{0.1}$. All Ca atoms lie near the center of 6-rings, and the electron density found in an 8-ring by earlier investigators is attributed to potassium scavenged during ion exchange. Approximately four-fifths of the Ca atoms (4.4 atoms per pseudocell) project into the large cage, and one-fifth (1.2 atoms) project into the sodalite unit. Both are bonded to three O(3) at about 2.3 Å. Electron density in the sodalite unit is attributed to Al in a tetrahedron of oxygen species, disordered into two orientations. All data are consistent with a cell content near $Ca_{5.3}Na_{0.4}Al_{11.0}Si_{13.0}O_{48}\cdot(Al_{0.3}O_{0.6}H_{0.3})$ in which the suggested H content is completely speculative.

A new determination of the crystal structure of dehydrated Sr-exchanged zeolite A[1] revealed Sr atoms only at the 6-rings and led to the suggestion that electron density found near the 8-rings in an earlier determination[2] actually resulted from introduction of potassium during ion exchange with impure solution. The present structure determination of dehydrated Ca-exchanged A provides a further test of this alternate interpretation to the now suspect claim of near-zero-coordination for divalent cations.[2,3] It also provides further evidence for an occluded tetrahedral complex produced during ion exchange with a divalent ion.

Experimental Section

Specimen Preparation. Crystals of zeolite 4A (Na-A) were prepared by a modification of Charnell's method[4] including a second crystallization using seed crystals from the first synthesis. Ion exchange at 95° C for 5 days with 1 M $CaCl_2$ solution (Alfa Optronic Grade 87607) resulted in occlusion of a chlorine species detected by electron microprobe analysis. Exchange at room temperature for 6 days, followed by thorough washing with deionized water, obviated occlusion of chlorine, but the crystals contained residual sodium. Exchange at room temperature for 2 weeks with two changes of water saturated with $Ca(OH)_2$ (Baker Analyzed Reagent 1372) yielded crystals of composition near $Na_{1.4}K_{0.7}Mg_{0.2}Ca_{4.6}Al_{11.6}Si_{12.4}O_{48}\cdot xH_2O$, and it was concluded that a trace of K, and perhaps Mg (but analyses near detection level), had been scavenged from the saturated solution which contains only 0.17 wt.% $Ca(OH)_2$ at 25 °C. Atomic absorption analysis of the saturated solution revealed the following weight ratios of Ca/Na/K/Mg: 97.9/1.7/0.4/<0.0002. Samples exchanged with 0.5 M solution of $Ca(ClO_4)_2$ (Alfa 22112) and an equal-volume mixture of 0.5 M $Ca(ClO_4)_2$ and saturated $Ca(OH)_2$ showed residual Na (~0.4 atom/48 oxygen) even after exchange for 2 months.

Crystals with properties given in ref 5 and 6 were selected for X-ray and electron microprobe measurements from the batch exchanged with

(1) Pluth, J. J.; Smith, J. V. *J. Am. Chem. Soc.* **1982**, *104*, 6977-6982.
(2) Firor, R. L.; Seff, K. *J. Am. Chem. Soc.* **1978**, *100*, 3091-3096.
(3) Firor, R. L., Seff, K. *J. Am. Chem. Soc.* **1978**, *100*, 978-980.
(4) Charnell, J. F. *J. Cryst. Growth* **1971**, *8*, 291-294.
(5) Pluth, J. J.; Smith, J. V. *J. Phys. Chem.* **1979**, *83*, 751-759.
(6) Pluth, J. J.; Smith, J. V. *J. Am. Chem. Soc.* **1980**, *102*, 4704-4708.

0002-7863/83/1505-1192$01.50/0